

Recombination in *a*-Si:H: Spin-dependent effects

R. A. Street

Xerox Palo Alto Research Center, 3333 Coyote Hill Road, Palo Alto, California 94304

(Received 18 January 1982)

Spin-dependent recombination in *a*-Si:H is studied using optically detected magnetic resonance (ODMR). Measurements are reported of the dependence of ODMR on temperature, illumination intensity, luminescence energy, microwave power, and defect density. Time-resolved ODMR using both transient illumination and transient microwave pulses are shown to be particularly informative. Samples with high-defect density exhibit a quenching spin-dependent effect which is identified with nonradiative recombination between unthermalized spins. The recombination is attributed to tunneling of band-tail electrons to dangling bonds. Low-defect-density samples have an additional quenching nonradiative mechanism, tentatively identified with Auger recombination, and a radiative enhancing process which we attribute to band-tail luminescence. The results support previous luminescence studies. We discuss the effects of microwave power, spin relaxation, and exchange on the ODMR results. The spin-lattice relaxation time T_1 and its temperature dependence are obtained from time-resolved ODMR and from ESR saturation measurements. Relaxation mechanisms are identified from the data.

I. INTRODUCTION

The recombination properties of hydrogenated amorphous silicon have now been fairly carefully investigated through luminescence measurements by a number of groups.¹ This author has proposed a model for the various recombination processes, a schematic diagram of which is shown in Fig. 1. The luminescence is dominated by a broad band at 1.3–1.4 eV, with a weaker transition at 0.8–0.9 eV present in some samples, notably doped material² and at measurements above 200 K.³ The 1.4-eV peak is believed to occur by tunneling of electron-hole pairs in localized band-tail states.⁴ The process is thought to be geminate at low-excitation intensity and low temperature, and nongeminate at high intensity.⁴ The width of the emission line has been attributed predominately to an electron-phonon interaction at the hole state.⁵ Lattice defects, specifically dangling bonds, have been identified as nonradiative recombination centers with the nonradiative mechanism being by direct tunneling at low temperature,⁶ and by ionization of the electron-hole pair followed by diffusion and capture at high temperature.⁷ Surface recombination⁸ and Auger recombination⁷ are also significant nonradiative mechanisms given appropriate experimental conditions.

Much of the evidence to identify the states in-

involved in the recombination comes from ESR data. The dangling bonds have the well-known resonance at $g=2.0055$.⁹ Light-induced ESR (LESR) has identified resonances at $g=2.004$ and $g \approx 2.013$ as electron and hole band-tail states, respectively.¹⁰ ESR measurements on doped *a*-Si:H support this interpretation.

Although the model depicted in Fig. 1 is generally successful in explaining most of the luminescence data, various aspects of the model require further confirmation. For example, the geminate process has also been questioned, and it has been suggested that dangling bonds are radiative rather than nonra-

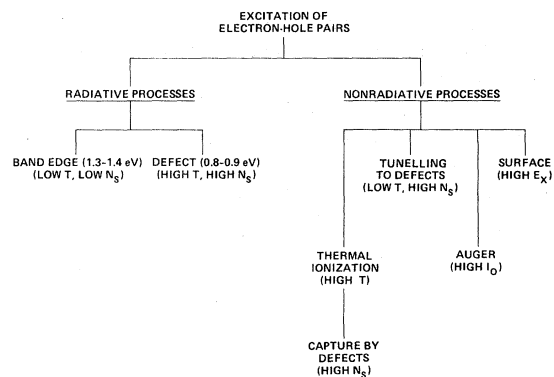


FIG. 1. Schematic diagram of the proposed recombination processes in *a*-Si:H (from Ref. 1).

diative centers.¹¹⁻¹³ Some of the evidence for the last two points comes from measurements of optically detected magnetic resonance ODMR, which is also the subject of this paper.

ODMR measures the change in luminescence output as a sample is brought into microwave resonance by the application of a magnetic field and microwave power.¹³ ODMR is of interest for *a*-Si:H for various reasons. One is its ability to link an ESR spectrum to a luminescence transition. Since each of the three states postulated in the recombination has an identifiable resonance line shape, it should be possible to positively identify the recombination mechanisms. In addition, it is found experimentally that the exchange interaction is weak so that the ODMR turns out to be closely related to the ESR line shapes. Undoubtedly, the weak exchange is related to the observed weak transition rates involved in the luminescence. Both are small because the states are localized and the wavefunction overlap is very small. ODMR is in principle a very sensitive test of the recombination models, because each has a very specific prediction for the spin dependence. For example, the geminate and nongeminate processes can give very different ODMR effects. It is also of general interest to understand and characterize the spin dependence, in particular the effects of spin relaxation and the transient ODMR.

There have been several studies of ODMR in *a*-Si:H which are discussed in more detail in Sec. V A. The early results identified three or four resonances corresponding to either a decrease or an increase in the luminescence intensity at resonance.^{14,15} The interpretation of the results was impeded by the limited amount of luminescence data at the time. More recent experiments have also been reported, although very different models have been proposed to interpret the results^{16,12,13,17,18} The problem seems to be one of properly identifying the ODMR resonances and their basic character (i.e., thermalized or unthermalized spins, etc.), and relating the results to known sample properties. In this paper we report studies of ODMR in samples of different defect density using time-resolved measurements to separate and characterize the resonances. In this way we believe that we can positively identify most of the ODMR effects, and we find that the results strongly support the recombination model outlined in Fig. 1.

In Sec. II the different experimental techniques are described. Sections III and IV describe the data and its interpretation for high- and low-defect-density samples, respectively. In Sec. V we compare

our results with others and discuss in more detail the time-resolved behavior, spin-lattice relaxation effects and microwave power saturation.

II. EXPERIMENTAL DETAILS

A. Apparatus and measurements

The spin-dependence measurements are made using a standard Varian X-band ESR apparatus equipped with a He gas flow cryostat and an optical access port to the cavity. The temperature range accessible is 12 K to room temperature. Luminescence is observed from the illuminated face of the sample and is detected perpendicular to the magnetic field by a cooled Ge detector with a response time of 300 nsec. The luminescence was dispersed with a grating monochromator to obtain the spectrum, but for measurements of the total luminescence output, the grating was replaced by a plane mirror. The excitation wavelength was 5145 or 6471 Å, and no significant difference in the results was observed for these two wavelengths. Four different types of spin-dependent measurements were made as follows.

(i) *cw measurements, field modulation.* In this experiment, the excitation light is kept on continuously. A small magnetic field modulation is applied at low frequency, usually less than 200 Hz, and the synchronous change in the luminescence intensity is measured using a lock-in detector. The magnetic field is then scanned slowly through the resonance. This measurement is analogous to the usual method for measuring ESR and results in a derivative spectrum. The advantages of field modulation are that the derivative spectrum allows structure to be identified more easily and allows a direct comparison with ESR line shapes. The majority of our cw measurements use this technique. The relative magnitude of $\Delta L/L$ is measured from the peak-to-peak amplitude of the derivative spectrum. An absolute calibration and confirmation of the sign of the effect was made by observing directly the change in the luminescence intensity.

(ii) *cw measurements, microwave modulation.* This is the method most widely used for spin-dependent measurements.¹⁴ The microwave excitation is chopped, and again the corresponding change in luminescence is measured using lock-in detection. This technique gives the spin-dependent response undifferentiated. We use a diode switch to chop the microwaves with a contrast ratio of about a factor of 10. In general, it is useful to perform both types of cw measurements as there can be a

real difference in the information obtained. The reason for this difference will become apparent in the discussion of microwave transient measurements. A problem with this technique is that two signals can have different phase relations to the modulation. In *a*-Si:H this occurs when the enhancing line and quenching line are present simultaneously (see Sec. IV), so that the relative intensities of the two lines depend on the choice of phase. However, the effect can also be used to separate the two lines.

(iii) *Light transient measurement.* This is one of two time-resolved spin-dependent measurements and detects the spin dependence of the component of luminescence emitted after a fixed delay time. The excitation light is pulsed using an acousto-optic modulator which can give light pulses from 50 nsec duration upwards at any chosen repetition rate. The time-resolved luminescence is measured using a box-car integrator. Once the pulse and gate have been set for a chosen delay time, the spin dependence is measured by modulating the magnetic field and using lock-in detection as in (i). The modulation frequency is set to be about an order of magnitude less than the excitation pulse repetition frequency (but in the present experiments it did not exceed 200 Hz) and is asynchronous. In these experiments it proved necessary to keep the repetition frequency low to minimize the background signal from the long decay components of the luminescence. In each case the background was measured by setting the gate to just before the excitation pulse.

(iv) *Microwave transient measurements.* This is a time-resolved measurement in which the excitation light is continuous and the response to a microwave pulse is measured instead. The experiment again uses a boxcar for the time resolution, and the output can be observed directly. However, to improve the signal by reducing base line drift, we have found it convenient to modulate the magnetic field and again use lock-in detection. This technique has another advantage in that if there are two overlapping signals, they can be fully separated by making measurements at the zero crossings of the two individual derivative spectra. To see this, suppose that the observed line $L(H)$ contains two derivative signals, $L(H) = A(H) + B(H)$, and that these have zero crossings at H_A and H_B [i.e., $A(H_A) = B(H_B) = 0$]. We also assume that only the intensity changes during the microwave transient, and the line shapes are unaltered. Then, if the transient measurement is performed at H_A , the data give the result for line B [since $L(H_A) = B(H_A)$] and vice versa.

Dunstan and Davies¹⁹ have shown that in general there can be two types of microwave transient effects, which are shown schematically in Fig. 2. In one case [Fig. 2(b)] there is an equilibrium change in the luminescence with a rise and decay time that depends on the recombination properties of the material. Alternatively, there may be a large transient change in luminescence with either no or a small equilibrium change [Fig. 2(a)]. As Depinna and Cavenett¹² point out, these types of response are very important for the interpretation of the data because they immediately distinguish between radiative and nonradiative mechanisms. To understand this, we note that the luminescence intensity L is given by

$$L = NP_R, \quad (1)$$

where N is the number of excited electron-hole pairs and P_R is the average radiative rate. N is governed by

$$dN/dt = G - N(P_R + P_{NR}), \quad (2)$$

where G is the generation rate and P_{NR} is the competing nonradiative recombination rate.

The ODMR experiment changes the transition rates P_R and P_{NR} , but N also responds through Eq. (2). Consider first a spin-dependent radiative process. When the microwaves are turned on, P_R changes in a time $\sim (\gamma H_1)^{-1}$, which is $\sim 10^{-7}$ sec in a typical experiment. (γ is the gyromagnetic ratio and H_1 is the oscillating magnetic field.) N responds in a time $(P_R + P_{NR})^{-1}$ which, in *a*-Si:H, is usually much longer, and the change in N is al-

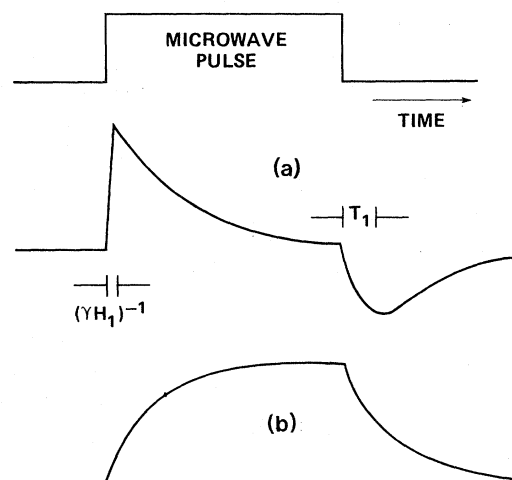


FIG. 2. Illustration of different types of microwave transient effects corresponding to radiative (a) and nonradiative (b) transitions.

ways in the direction of restoring L towards its previous value. Thus, the response is as in Fig. 2(a). At the end of the pulse, the effective P_R changes and N again responds through Eq. (2). If the relaxation time T_1 is sufficiently short, there is a negatively going transient with time constant T_1 followed by a recovery with time constant $(P_R + P_{NR})^{-1}$, which is the condition indicated in Fig. 2(b). If, on the other hand, T_1 is longer than the recombination time, the transient shape is unchanged but the two time constants are interchanged.

The results are completely different when only the nonradiative channel is spin dependent. Changes in L occur only through N and are governed by Eq. (2). The response time is therefore slow, of order $(P_R + P_{NR})^{-1}$, and there is no transient spike as in Fig. 2(b). The sudden transient is therefore a signature of a radiative process.

This property of a transient response can also lead to a different result in the two cw measurements, (i) and (ii). The transient is observed in a microwave chopping experiment, but the signal will not be completely in phase with the microwaves. No signal at all will be observed with field modulation if the modulation amplitude is less than the spin-packet width. However, this is generally not the case. Instead, as the field sweeps through the spin packet, the effect will be that of a short microwave pulse, and so the ODMR line will be observed.

B. Samples

The samples of *a*-Si:H, deposited on 7059 glass substrates, were made by plasma decomposition of SiH₄ as has been described in detail elsewhere.⁶ It is well known that by varying the deposition conditions (substrate temperature, rf power, etc.), samples of different spin density ranging from $\sim 3 \times 10^{15}$ up to $\sim 10^{19}$ cm⁻³ can be produced. The ESR is the usual 7.5 G line at $g = 2.0055$ which has been identified as a dangling bond.²⁰ We have also shown previously that the spin density and the luminescence are closely correlated in that a spin density of greater than 10^{17} cm⁻³ results in strong quenching of the luminescence.⁶ Our first experiments were therefore to observe the spin-dependence $\Delta L/L$ in samples of varying spin density, and a selection of these results are shown in Fig. 3. The data include the illumination intensity dependence and are measured at 85 K. These cw measurements use a magnetic field modulation of 5 G, and in all cases a

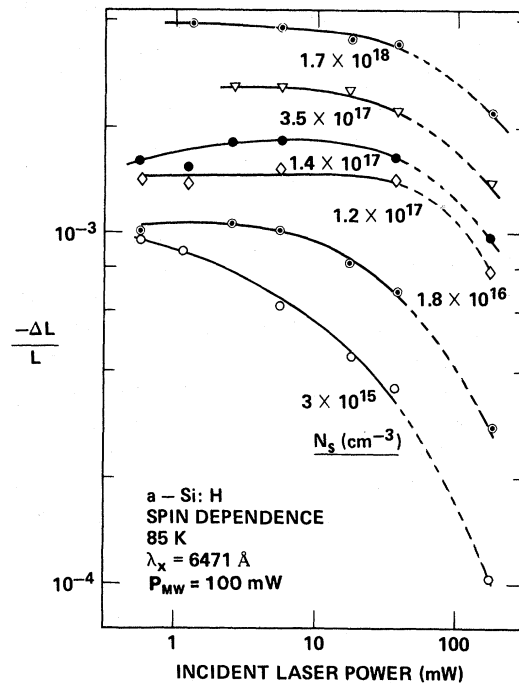


FIG. 3. Plot of the spin-dependence $\Delta L/L$ vs illumination intensity for samples of different spin density. At the highest intensity, $\Delta L/L$ is artificially reduced by heating effects.

quenching signal is observed. We observe two different types of behavior depending on spin-density N_s . In samples with N_s greater than 10^{17} cm⁻³, $\Delta L/L$ is independent of illumination intensity and increases monotonically with N_s . The decrease in $\Delta L/L$ seen at the highest intensity is an artifact caused by sample heating which was confirmed by observing a transient decrease in the luminescence immediately after illumination. When N_s is substantially above 2×10^{18} cm⁻³, $\Delta L/L$ decreases again. However, these samples have very weak luminescence and were not studied further. Samples with N_s less than 10^{17} cm⁻³ show a pronounced light intensity dependence which cannot be ascribed to heating. In addition, the shape of the resonance spectrum changes with intensity as is described in more detail in Secs. III and IV.

Since a spin density of $\sim 10^{17}$ cm⁻³ corresponds both to the onset of luminescence quenching and to a change in the spin-dependence properties, this provides a natural division of the samples, and below we investigate these two regions separately. We present in Sec. III detailed data for a sample with $N_s = 3.5 \times 10^{17}$ cm⁻³ which typifies the high-defect-density material. This sample was chosen

because it has the maximum signal-to-noise in $\Delta L/L$, corresponding to a compromise between an increasing $\Delta L/L$ and decreasing L . A study of the high-defect-density material is also reported elsewhere.¹⁸ To examine the low-defect-density regime, we studied a sample with $N_s \sim 3 \times 10^{15} \text{ cm}^{-3}$. No equilibrium ESR was detected in this sample; instead, the spin density was established from a sample of identical deposition conditions deposited on Al foil and chemically removed. Data on this sample are reported in Sec. IV. In each case some measurements were made on other samples to confirm that the behavior was properly representative. The luminescence spectra of the two samples are shown in Fig. 4. These spectra confirm that the luminescence is a single broad band at 1.3–1.4 eV. No significant emission from the 0.9 eV defect peak is found.

III. HIGH-DEFECT-DENSITY MATERIAL

Figure 5 shows the cw ODMR spectrum of the high-defect-density sample obtained using field

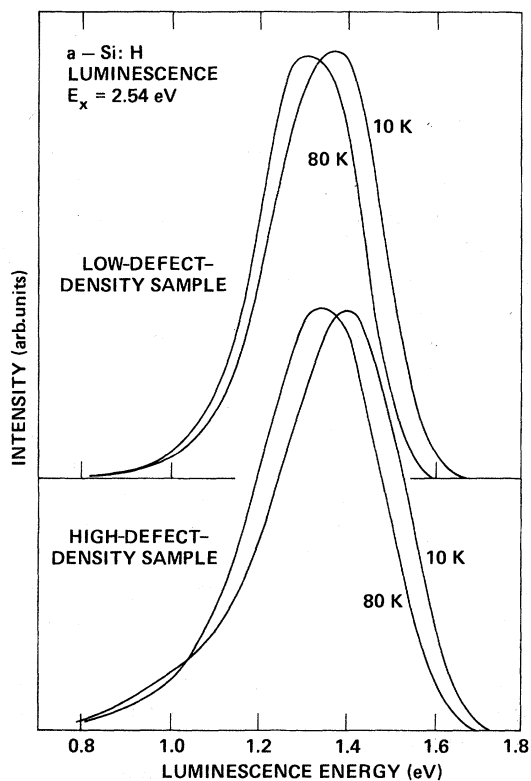


FIG. 4. Luminescence spectra at 10 and 80 K of the two samples from which most of the ODMR data was taken.

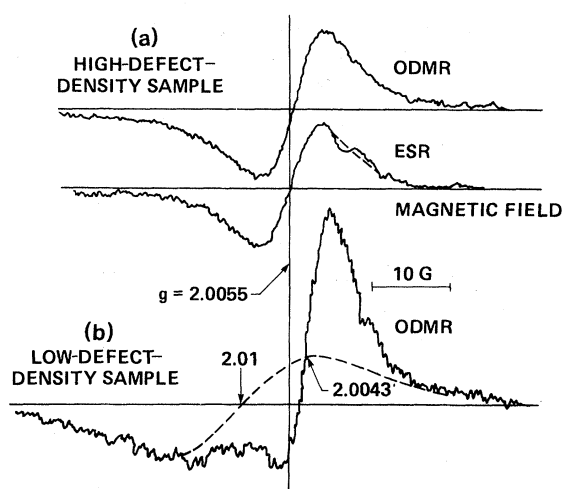


FIG. 5. ODMR quenching resonances in the high-defect-density and low-defect-density samples at 85 K. The direct comparison with the ESR resonance is shown for the high-defect-density sample.

modulation. The same figure also shows the conventional derivative dark ESR spectrum. The two sets of data were taken sequentially, keeping the temperature (85 K), the modulation amplitude (5 G), and modulation frequency (150 Hz) constant. Only the microwave power was changed because at the low power at which ESR saturation occurs, the ODMR signal is very weak. Figure 5 shows that the two resonances are very similar, apart from the substrate resonance seen on the high-field side of the ESR. (This signal is observed in the substrate without a deposited *a*-Si:H film.) The ODMR has a lower g value by about 0.003, and the peak-to-peak widths are the same within experimental uncertainty. The g values are listed in Table I.

Figures 6 and 7 show some characteristics of the cw spin dependence. The spectral dependence (Fig. 6) shows that $\Delta L/L$ increases on the low-energy side of the luminescence spectrum, but there is no change in the shape of the resonance. The shape of the $\Delta L/L$ spectrum changes with temperature, although the qualitative behavior is preserved, at least over the limited range investigated. The temperature dependence of $\Delta L/L$ for the total luminescence intensity is shown in Fig. 7. There is a steady decrease in $\Delta L/L$ by a factor ~ 20 as the temperature is raised to 230 K. Over the same range, L decreases by almost a factor of 100. Again, there is no discernible change in the shape of the ODMR line shape.

These experiments characterize the spin dependence, but are not very informative in understand-

TABLE I. G values of ODMR obtained by a direct comparison to ESR (or LESR) on the same sample. For purposes of calibration it is assumed that the dangling bond ESR is at $g = 2.0055$ and the narrow LESR line is at $g = 2.0045$.

		g values	
High defect	ESR		2.0055
Density sample	ODMR	Q_1	2.0052 ± 0.0003
Low defect	ESR		$2.0045, 2.011 \pm 0.001$
Density sample	ODMR	Q_1	2.0055 ± 0.0005
	ODMR	Q_2	$2.0045 \pm 0.003, 2.011 \pm 0.001$
	ODMR	E_1	2.0085 ± 0.001

ing the effect. The problem is that there are many variables that can change with temperature and luminescence energy, such as the distribution of luminescence lifetimes, the spin-lattice relaxation time, and the radiative and nonradiative mechanisms. We have found that the time-resolved measurements are more valuable for understanding the spin-dependent mechanisms.

Figure 8 shows the result of light transient measurements at different temperatures.¹⁸ Each set of data corresponds to a series of different pulse lengths, gate widths, and repetition rates. Usually the pulse and gate were set equal, and the delay ranged from 1 to 10 times the pulse width. The repetition rate was chosen such that the background signal, measured just before the pulse, was small compared to the signal within the luminescence decay. The luminescence decay extends over a broad time range with distributed decay times, and this allows measurements of $\Delta L/L$ from 10^{-6} to about 10^{-2} sec. $\Delta L/L$ is observed to increase logarithmically with time at sufficiently short times (see Fig. 8), and in this region $\Delta L/L$ is essentially indepen-

dent of temperature. The maximum $\Delta L/L$ at low temperature and long delay corresponds to about a 4% change in the luminescence intensity. There is a cutoff in $\Delta L/L$ which occurs at a time that is strongly temperature dependent. The cutoff is at $\sim 10^{-4}$ sec at 125 K but increases to above 10^{-2} sec at 13 K.

Figure 9 shows the dependence of the time resolved $\Delta L/L$ on microwave power p_{MW} . The qualitative behavior, that of a slightly sublinear dependence on $p_{MW}^{1/2}$, is seen in all the cw measurements too. In the time-resolved measurements, there is a tendency toward greater saturation at the long time constants. For this reason the shape of the data in Fig. 8 is sensitive to the choice of microwave power, although the qualitative behavior will not change. The microwave saturation properties will be discussed in Sec. V B.

Figure 10 shows the results of microwave transient measurements. There is a slow onset of the

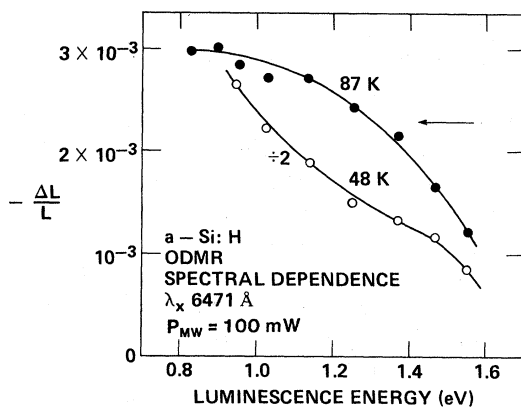


FIG. 6. Spectral dependence of $\Delta L/L$ for the high-defect-density sample at two temperatures. The arrow indicates the value of $\Delta L/L$ for the total luminescence at 87 K.

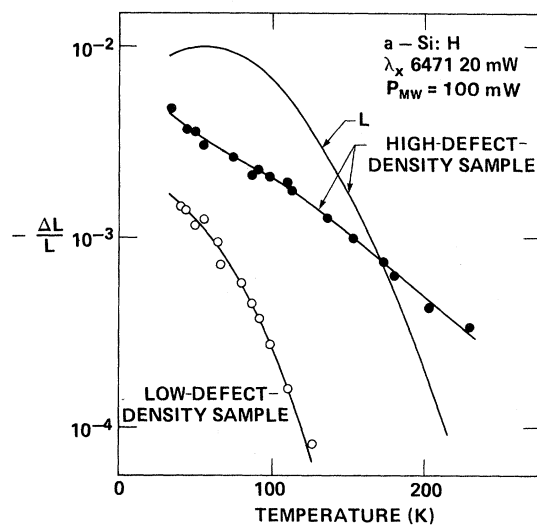


FIG. 7. The temperature dependence of $\Delta L/L$ for the quenching lines in the high-defect-density and low-defect-density samples. L is the relative luminescence intensity.

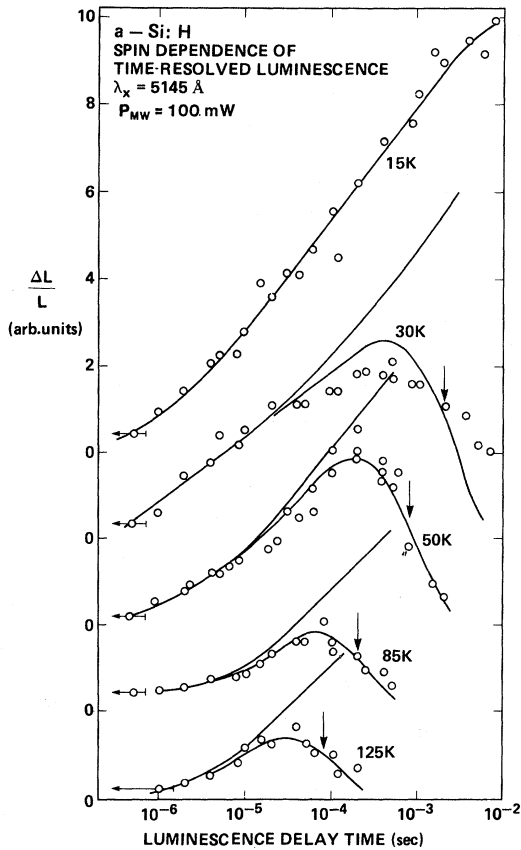


FIG. 8. Results of light-transient time-resolved ODMR at different temperature. The solid lines are a fit to the data assuming a spin-lattice relaxation time, as indicated by the arrow, using a procedure described in Ref. 18.

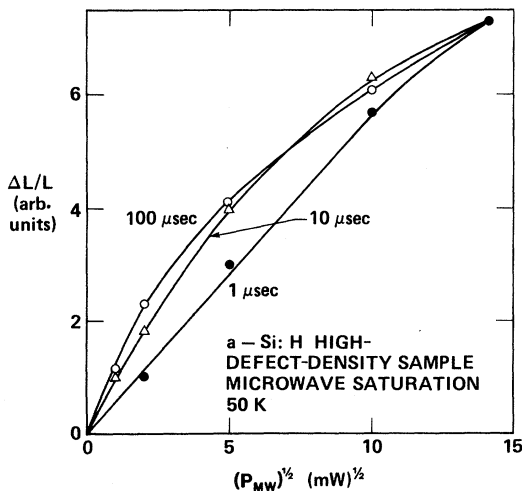


FIG. 9. Plot of the time-resolved $\Delta L/L$ vs microwave power P_{MW} showing the saturation effects at different delay times as indicated.

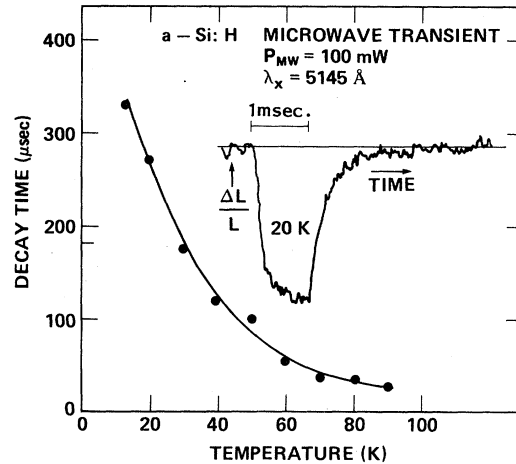


FIG. 10. Results of microwave transient time-resolved measurements on the high-defect-density sample. The decay times are obtained by fitting the initial decay to an exponential law.

spin dependence reaching an equilibrium change in L without any initial transient. The decay has an identical time constant within the experimental uncertainty, and the time constant of the initial decay decreases from $\sim 300 \mu\text{sec}$ at 15 K by about an order of magnitude at 90 K, as is also shown in Fig. 10. The shape of the transient response agrees with the similar observations by Depinna and Cavenett.¹³

A. Interpretation of the results

The sample with a high-defect density has been discussed first because the results are relatively straightforward, since the same ODMR line shape is observed in all the experiments. The interpretation of the data is also discussed elsewhere.¹⁸ We believe that the cw spectral dependence (Fig. 6) and temperature dependence (Fig. 7) can be readily understood in terms of the light-transient data. It is known that the high-energy side of the luminescence spectrum has a larger contribution from short decay times than the low-energy side.⁴ As seen in Fig. 8, these short-time constants contribute very little to $\Delta L/L$ and so account for the observed spectral dependence. The decrease in $\Delta L/L$ with temperature is clearly related to the temperature dependence of the cutoff in $\Delta L/L$ seen in Fig. 8. We conclude that $\Delta L/L$ is actually insensitive to temperature, provided the spin dependence occurs at times shorter than the cutoff time. The actual

cw temperature dependence will also depend on the change in the distribution of luminescence lifetimes with temperature, so would be difficult to compute accurately from Fig. 8. This discussion demonstrates that the spectral and temperature dependence by themselves are not good indicators of the ODMR properties because of the distribution of decay lifetimes in *a*-Si:H. The time-resolved data gives much more precise information.

The absence of significant temperature dependence and large magnitude of $\Delta L/L$ in the time-resolved measurements below the cutoff time show that the spins are unthermalized, as is pointed out elsewhere.¹⁸ The cutoff is then interpreted as the appropriate spin-lattice relaxation time T_1 , since when T_1 is exceeded, $\Delta L/L$ is expected to drop to nearly zero. The solid lines in Fig. 8 show a fit to the data from which T_1 is obtained.¹⁸ This model is confirmed by measurements of T_1 from the ESR saturation of the dangling bond by resonance, which are discussed in Sec. V E. In addition, in Sec. V C, we calculate the expected time dependence of $\Delta L/L$ before the T_1 cutoff using the recombination models developed for *a*-Si:H and obtain good qualitative agreement with the data in Fig. 8.

The microwave transient data clearly identifies the effect as arising from a nonradiative transition because there is no rapid microwave transient. The data is of the form in Fig. 2(b) rather than Fig. 2(a).

In order to interpret the ODMR resonance more specifically, we note the following observations. The ODMR signal is associated with samples with a dangling-bond spin density greater than 10^{17} cm^{-3} . The ODMR is very similar to the dangling-bond ESR line shape. Our previous model explained the decrease in luminescence intensity as the dangling-bond density is increased above 10^{17} cm^{-3} in terms of nonradiative tunneling from the conduction-band tail to the dangling bonds. In general, in the limit of weak exchange, the ODMR should comprise the two resonances of the recombining particles. The recombination model of tunneling to dangling bonds predicts an ODMR spectrum which is the sum of the known $g=2.0055$ (dangling bond) and the $g=2.0045$ (band-tail electron) resonances. Unfortunately, the two resonances are too close to expect them to be resolved in the ODMR. However, within experimental uncertainty, the ODMR line is consistent with the sum of these two resonances, and the small shift in the ODMR g value below 2.0055 is perhaps a manifestation of the presence of the 2.0045 line. Lastly, we note that this recombination model predicts a quenching effect,²¹ as observed.

IV. LOW-DEFECT-DENSITY MATERIAL

The low-defect-density sample was found to have more complex spin-dependent effects than the high-defect-density material, having three identifiable ODMR lines. An indication of the complexity is shown by the light-intensity dependence data in Figs. 3 and 11. At 85 K only quenching ODMR is observed and $\Delta L/L$ decreases as the excitation intensity increases and is accompanied by a change in line shape. At low intensity, the line is very similar to the dangling-bond resonance observed in the high-defect-density material. At high illumination levels, there is a change to a two-component resonance in which the low g -value component (2.0045) is narrow and the high g -value component (2.011) is broader (see Fig. 5). We shall refer to this pair of quenching lines as Q_2 and the dangling-bond related resonance as Q_1 .

At 15 K the data are very different. A quenching line is still observed at high excitation intensity but $\Delta L/L$ for these lines decreases steadily at lower intensity. In addition, there is an enhancing line E_1 at $g \approx 2.009$ with width ~ 17 G. $\Delta L/L$ for this line increases slowly as the illumination intensity decreases. Because of the overlap of the two lines, it is impossible to determine whether the quenching resonance is Q_1 or Q_2 .

The spectral dependences of all three lines are similar to that found in the high-defect density, with $\Delta L/L$ decreasing at high energy. The temperature dependence of the quenching line is shown in Fig. 7. The quenching lines decrease more rapidly than in the high-defect-density sample and become undetectable above 125 K. E_1 also decreases rapidly and is unobservable above 50 K.

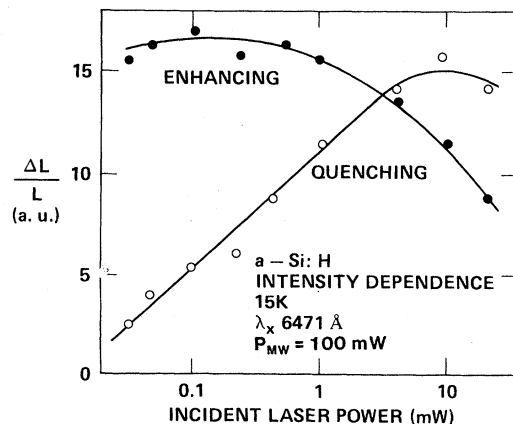


FIG. 11. Plot of the illumination intensity dependence of the quenching and enhancing lines in the low-defect-density sample at 15 K.

As before, the transient measurements clarify the data, and results are shown in Figs. 12 and 13 for various temperatures. In each case there is an interesting characteristic behavior. We can define two times t_A and t_B , which divide the time response into three zones. At short times, less than t_A , we observe the quenching line Q_2 . For this line $\Delta L/L$ increases with delay time up to the cutoff at t_A . Below the temperature-dependent cutoff, the magnitude of $\Delta L/L$ is approximately independent of temperature. The behavior is therefore qualitatively similar to that of Q_1 in the high-defect-density sample except that the cutoff occurs at much shorter times (compare Fig. 12 and Fig. 8). These measurements provide the clearest line shape of Q_2 and so we take the opportunity to compare the spectrum with ESR, and both are shown in Fig. 13 with the g values given in Table I. In this case, the measurement is of light-induced ESR,¹⁰ there being no detectable dark signal. The comparison in Fig. 13 shows a striking similarity in the data, both line

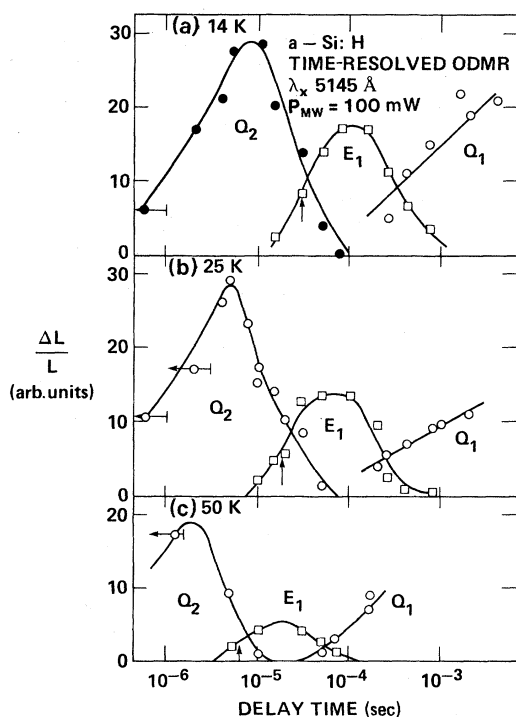


FIG. 12. Results of light-transient time-resolved measurements in the low-defect-density sample at different temperatures. $\Delta L/L$ is measured from the peak-to-peak height of the derivative resonances. Correcting for the different widths of the resonances would increase the magnitude of E_1 by a factor of 8, and Q_1 by a factor ~ 1.5 compared to Q_2 . The arrows indicate the time at which E_1 reaches half its maximum intensity and is taken as the measure of T_1 (see text).

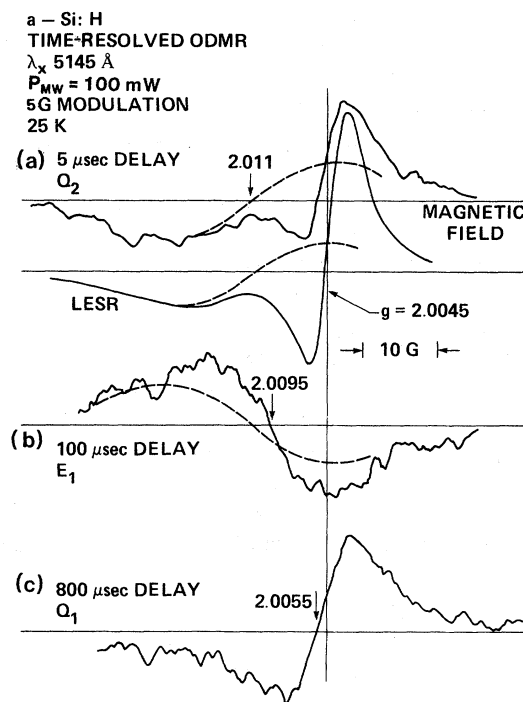


FIG. 13. Typical ODMR resonances of Q_2 , E_1 , and Q_1 taken from the 25-K time-resolved data on Fig. 12. The quenching line Q_2 is compared with light-induced ESR data in the same sample. Both lines show the estimated deconvolution of the spectra into the band-tail electron and hole lines as in Ref. 10. The same band-tail hole line is compared to the E_1 ODMR in (b).

shapes having two components of similar g value and linewidth. The lines are also clearly distinguishable from the dangling-bond resonance. The relative intensity of the two lines is different in ODMR and ESR, but since they saturate differently, this is not too surprising.

When the delay time exceeds t_A , Q_2 disappears and is replaced by E_1 (Figs. 12 and 13). E_1 in turn disappears at t_B , and at longer times a quenching line is again observed. As shown in Fig. 13, this line has a similar g value and width of the ODMR in the high-defect-density samples, as well as a similar time-resolved behavior. We therefore identify this as Q_1 . It should be noted that the time-resolved data show clearly the different properties of Q_1 and Q_2 . This characteristic time-resolved behavior is observed at temperatures between 15 and 50 K. Over this range, the times t_A and t_B decrease approximately inversely with temperature.

The microwave transient measurements at 15 K are shown in Fig. 14 using the zero-crossing technique discussed in Sec. II A (iv). We obtained the

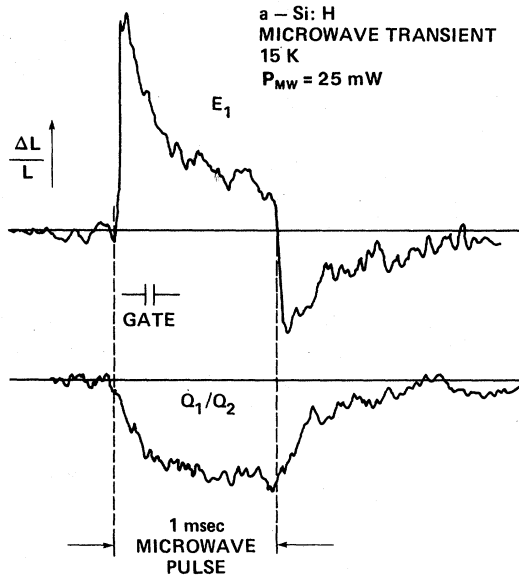


FIG. 14. Results of microwave transient time-resolved measurements on the low-defect-density sample. The two sets of data are measured at the zero crossings of the two components of the derivative ODMR lines, to isolate the different transient responses.

zero crossing of the component resonances Q_1/Q_2 and E_1 by measuring the ODMR at different parts of the pulse. (Again we are unable to unambiguously determine whether the quenching line is Q_1 or Q_2 because of the overlap with E_1 and because of the very small difference in the zero-crossing position for these two lines.) The transient response for both components could then be isolated and are shown separately in Fig. 14. It is readily seen that the two responses are different and correspond to the two types shown in Fig. 2. Thus Q_1/Q_2 has a slow rise to an equilibrium change in L and a decay with the same time constant, as was found for the quenching line in the high-defect-density material. On the other hand, E_1 has a fast transient at the start and end of the microwave pulse with no detectable change in L at the end of the pulse.

Table I shows the g values of the ODMR lines observed in low-defect-density material. Since Q_2 can be resolved into two components, these g values are shown separately. The values quoted are obtained from comparing a large number of ODMR spectra taken under different experimental conditions, chosen to optimize the observation of each line. For example, E_1 can be seen clearly in the time-resolved microwave pulsing measurements by setting the gate at the start of the pulse (see Fig. 14),

or in cw measurements at low intensity (see Fig. 11). The g values and estimated uncertainties given in Table I are taken from a mutually consistent fit of the various data using the three-component ODMR lines.

A. Interpretation of the data

As before, the time-resolved measurements give the most precise ODMR information. The temperature and spectral dependence of the cw measurements are again consistent with the time-resolved data when account is taken of the changes in the distribution of decay times. In general, we shall see that the interpretation of the ODMR is less certain than in the previous case, although a reasonably strong case can be made for the model proposed here, which is in fact based on our previous luminescence data.

Q_1 line. We interpret Q_1 as the dangling-bond process observed in high N_s samples because of its g value and line shape as well as the light-transient data which are similar to the results in Sec. III. The magnitude of $\Delta L/L$ for this line is less than for the high-defect-density sample, as expected from the lower defect density and the relatively minor role of nonradiative recombination at low temperature. However, it is known that above 50 K, dangling bonds, even in low density, play an important role in nonradiative recombination by a process of diffusion and capture.⁷ Possibly this mechanism is the origin of the different intensity dependences shown in Figs. 3 and 11.

Q_2 lines. The Q_2 pair of lines is distinctly different from Q_1 in both ODMR line shape and in the time dependence of the cutoff. Q_2 therefore cannot be identified as the dangling bond. Instead, the ODMR closely resembles the light-induced ESR (see Table I), which we (and others) have identified as the electron and hole band-tail states.¹⁰ Q_2 has a time dependence characterized by a temperature-independent $\Delta L/L$ at short times and a temperature-dependent cutoff. As discussed for Q_1 , this is the signature of a pair of unthermalized spins, with the cutoff occurring at the appropriate spin-lattice relaxation time T_1 . As discussed further in Sec. V E, the cutoff in Q_2 is determined by the hole state. Q_1 does not involve holes, and in this case the cutoff is determined by the dangling bond T_1 , which is much longer.

It is very tempting to interpret Q_2 as geminate radiative recombination of an electron-hole pair, since this mechanism predicts a quenching ODMR

process with the observed line shape. However, this does not seem to be possible as the microwave pulsing measurements characterize Q_2 as a nonradiative transition (Fig. 14), although there is some ambiguity as to the relative contributions of Q_1 and Q_2 in this experiment. We therefore suggest an alternative explanation. Previous luminescence measurements have shown that in low-defect-density material at low temperature, Auger recombination is an important mechanism.⁷ In fact there is substantial evidence supporting the interpretation of the Q_2 lines as originating from the Auger process. First, the onset of Q_2 with increasing light intensity (Fig. 11) occurs near the known transition from monomolecular to bimolecular recombination kinetics, which is also associated with the onset of the Auger process. Second, the light-transient measurements show that Q_2 only occurs coincident with the excitation pulse or at short delay times. This corresponds to conditions when there is the highest density of excited electron-hole pairs. Third, the ODMR line shape leads us to identify the two resonances as conduction band-tail electrons and valence band-tail holes, which are the states participating in the Auger process.

E_1 line. The transient microwave response of the E_1 line associates it with the radiative transition without any need for a competing nonradiative process. This interpretation is supported by the fact that it is the only line observed in cw measurements in the limit of low-defect density, low excitation intensity, and low temperature. These conditions are known to isolate the radiative process. Our proposed interpretation of the enhancing line differs in two major respects from previous suggestions. Firstly, two enhancing lines have previously been identified, a relatively narrow one (20 G) and a very broad one (200 G).^{15,16} As discussed in Sec. VB, we believe the broad wings to the E_1 spectrum are simply the effect of microwave power broadening. Similar wings are in fact seen in Q_1 , and the broadening is consistent both with an estimate of the effect and with the observed dependence on microwave power. Secondly, the enhancing line has been interpreted as from thermalized spins from the T^{-2} temperature dependence of the cw ODMR.¹⁵ We now see that this experiment can be ambiguous because of the time-dependent effects. In the time-resolved measurements we find that $\Delta L/L$ in fact decreases much slower than T^{-2} . Our interpretation is that E_1 occurs with one spin thermalized and one unthermalized. The justification of this model is based on the time dependence and is discussed in Sec. VD.

The interpretation of the E_1 ODMR in terms of a recombination model presents some difficulties. The g value is ~ 2.0085 and peak-peak width 15–20 G. This compares with the ESR hole line which is even broader and has a larger g value, or with the electron or dangling bond ESR, both of which are much narrower and at lower g value. Our luminescence model would suggest that E_1 should comprise the band-tail electron and hole resonances. These two resonances are sufficiently different that they could easily be resolved, as indeed they are in Q_2 . There seem now to be two possibilities. One is that the E_1 radiative transition is comprised of new states which have not yet been identified in ESR. The second alternative, which we prefer, is that the electron and hole band-tail states are present in E_1 but with modified line shape. An obvious possibility is that a weak exchange interaction is present. This results in a line shape which is roughly the average of the electron and hole ESR. The g value would then be $2.008 [\frac{1}{2} (2.0045 + 2.011)]$, which is indeed close to the observed value. We suggest the following explanation of why the exchange interaction is apparently only observed in the radiative process. The recombination time in a tunneling process is given by $\tau_0 \exp(2\alpha R)$. The exchange energy should be roughly proportional to the overlap term $\exp(-2\alpha R)$. For nonradiative tunneling $\tau_0 \sim 10^{-12}$ sec, whereas for the radiative process $\tau_0 \sim 10^{-8}$ sec. Thus for the same decay time, the radiative process requires a much larger term than the nonradiative process. We do not have an estimate for the prefactor of the Auger process, but assume that it must be sufficiently short to make exchange negligible despite the short recombination times.

In summary, we have developed an interpretation of Q_1 , Q_2 , and E_1 which accounts for all our ODMR data. Some aspects of the data are evidently open to alternative interpretation, and further experimental evidence would be valuable. However, the model is developed entirely in terms of recombination processes for which other evidence has already been reported. We therefore conclude that the ODMR results support the general recombination model for α -Si:H which was described briefly in the Introduction.

V. DISCUSSION

It should be evident from Secs. III and IV that the interpretation of ODMR presents a problem at two levels. One is the general characterization of

the effects in terms of thermalized or unthermalized spins and radiative or nonradiative processes. The second is an interpretation of the resonances in terms of identifiable states in the material. Most of this section is devoted to a detailed discussion of various aspects of the first problem. Based on this discussion, we believe that the effects can be characterized with confidence. It should be recognized that our conclusions are very different from those given by others. For example, we find two quenching effects and one enhancing, whereas others find one quenching and two or even more enhancing lines. The differences in interpretation are discussed in Sec. V A.

A. Comparison with other data

Several studies of spin-dependent luminescence in α -Si:H have been reported. Recently Depinna and Cavenett have observed a pair of quenching lines and four enhancing lines from both glow discharge and sputtered α -Si:H at 2 K.^{13,16} The quenching lines resemble the pair Q_2 that we observe, as the line is asymmetric on the low-magnetic field side. The microwave transient waveform also agrees with ours. Their enhancing lines differ in detail from ours. A very striking difference in the data is the excitation intensity dependence. Depinna and Cavenett report that at 2 K, as the intensity increases the line changes from quenching to enhancing. Our data at 15 K show exactly the opposite, and the reason for this difference is not clear. Depinna and Cavenett have a model which is very different from ours to explain the data. They suggest that dangling bonds are radiative centers, and that the dominant luminescence band at 1.3–1.4 eV in fact comprises two bands at 1.4 and 1.25 eV. We believe that the evidence for nonradiative dangling bonds is extremely strong, as described in Sec. III and elsewhere.¹⁸ Depinna and Cavenett evidently did not have access to samples in which N_s could be varied, and this makes it difficult to identify the dangling bonds properly. We also do not find evidence for two luminescence bands, but instead interpret the spectral dependence in terms of the different distributions of luminescence decay times that are known to occur across the spectrum. However, since Depinna and Cavenett used different samples from ours, the possibility that their luminescence spectra contain an extra band cannot be easily ruled out.

Morigaki *et al.* have also reported recent ODMR data.¹⁷ They also find a pair of quenching lines

with roughly similar g values as our Q_2 pair, although the line shape is different. However, almost certainly the different line shape is due to an interference with enhancing lines. They find an enhancing line similar to ours, although the line is very heavily weighed to the low end of the luminescence spectrum, unlike ours. They interpret the broad wings to the enhancing line as a second acceptorlike state rather than power broadening of the line. Morigaki *et al.* interpret one of the quenching lines as dangling bonds, but without knowing the spin density of the sample or the exact line shape, it is hard to confirm this result. They interpret the data in terms of radiative band-tail states and nonradiative dangling bonds in general agreement with our model. However, various details of the model are different. For example, they propose a very broad conduction band tail which directly conflicts with transport measurements. Also, they assume a very strong electron-phonon interaction (of order 1 eV) at the dangling bonds for which we see little justification.

We have previously reported spin-dependent luminescence on α -Si:H using microwave modulation.¹⁵ We also observed a pair of quenching lines, one of which we identified as the dangling bond. The present results indicate that this is not correct, and that the pair Q_2 or a combination of Q_1 and Q_2 was in fact observed. Our previous results found that the quenching lines were independent of temperature up to ~ 100 K, which differs from the present data. The reason for this difference is probably that we were using a Si diode detector with a cutoff at ~ 1.2 eV. Figure 6 shows that the spectral dependence gets less strong at high temperature, thus increasing $\Delta L/L$ on the high-energy side of the spectrum.

Clearly there are substantial differences in the reported data. However, since the ODMR spectrum depends on the spin density, temperature, wavelength, microwave power, light intensity, etc., this is not too surprising. In each report the quenching lines look qualitatively similar, although we now find that the dangling-bond signal is distinct from the Q_2 pair which arises from band-tail states.

B. Microwave saturation

$\Delta L/L$ is observed to increase with microwave power up to 200 mW in Fig. 9, with little sign of saturation. In contrast, the dangling-bond ESR at 50 K is saturated at 10^{-3} mW. Previously, we assumed that the higher saturation power occurred because the effective T_1 was reduced by the

luminescence decay time. However, since T_1 is the same magnitude as the longest delay time shown in Fig. 8, this explanation is clearly incorrect.

In fact, the different dependence on microwave power occurs because of the different nature of the experiment. The ODMR is observed when there is a high probability of a spin flip during the appropriate measurement time. $\Delta L/L$ is therefore proportional to the probability $P(t)$ that the particle is in a state $+\frac{1}{2}$ at time t if it was in state $-\frac{1}{2}$ at time zero. Hyde²² has shown that in saturation, the averaged P is given by

$$P = \pi h(H - H_0) \gamma H_1 / 2, \quad (3)$$

where h is the shape function of the line. The calculation is made assuming an inhomogeneous line with T_1 and $T_2 \gg (\gamma H_1)^{-1}$, which is appropriate to α -Si:H. Note that the ODMR is proportional to P , while the ESR signal is given by P/H_1 . Thus for an inhomogeneous line, the ESR is independent of microwave power p_{MW} in saturation, whereas the ODMR should be proportional to $p_{MW}^{1/2}$ until the spin-packet width exceeds the inhomogeneous linewidth. The data of Fig. 9 show this behavior and incidentally confirm that the dangling bond line is inhomogeneously broadened.

Davies²³ has shown that ODMR from an inhomogeneous line can be enhanced by applying a high-frequency magnetic field modulation. The reason is that provided the microwave power is high enough, spins throughout the width of the modulation can be brought into resonance simultaneously. We observe enhancement for each of the ODMR lines, showing that all these are inhomogeneously broadened. The enhancement depends on microwave power and modulation frequency in general agreement with the predictions of Davies. The maximum effect observed is about a factor of 5.

Another process influencing the ODMR is the broadening due to the microwave field. This has received little attention, and we believe it has caused an erroneous identification of an ODMR line in α -Si:H. ODMR is generally performed at high microwave power to maximize the signal, as discussed above so that over most experimental conditions, the spin-packet width is determined by H_1 . Under these circumstances the magnetization is given by²⁴

$$M_x(H) = M_0 \int \frac{h(H_i - H_0) dH_i}{[1 + (H_i - H)^2 / H_1^2]^{1/2}}, \quad (4)$$

where $h(H)$ is the normalized shape function of the inhomogeneous line. From Eq. (4) we find that at the center of the resonance ($H = H_0$),

$$M_x(H_0) \simeq 2M_0 h(0) H_1 \ln(2\Delta/H_1), \quad (5)$$

where Δ is the approximate width of $h(H)$. [$2\Delta h(0) = 1$.] Far from the center of the resonance ($|H - H_0| \gg \Delta$),

$$M_x(H) \simeq \frac{M_0 H_1}{H_0 - H} \quad (6)$$

$$\simeq \frac{M_x(H_0) \Delta}{(H_0 - H) \ln(2\Delta/H_1)}. \quad (7)$$

It can now be seen that the line has wings that extend surprisingly far in magnetic field. The intensity of the wings also is expected to decrease logarithmically with decreasing H_1 .

In Fig. 15 we show the ODMR line shapes for the Q_1 and E_1 lines using the microwave chopping technique. In each case the line contains broad wings that are observable out to at least 200 G from the center. The relative amplitude in the wings decreases with H_1 qualitatively as predicted by Eq. (7). Figure 15 also shows the result of a numerical integration of Eq. (4) for a Gaussian line shape and illustrates the wings of the resonance introduced by power broadening. The broadening is sensitive to the choice of line shape (i.e., Gaussian or Lorentzian). The calculations show that power broadening

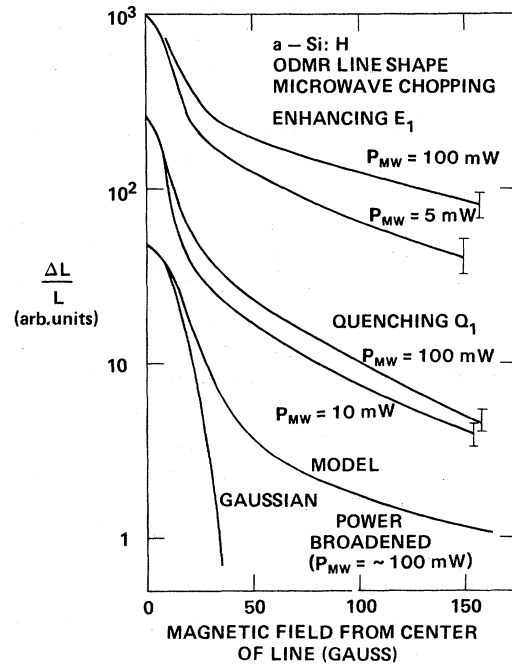


FIG. 15. ODMR line shape measured by microwave chopping for E_1 and Q_1 showing the broad tail that extends about 200 G. Also shown is a model calculation of power broadening of a Gaussian line.

can account for the line shape of the data, and that there is no indication of a broad enhancing ODMR signal.

C. Time-resolved ODMR when both spins are thermalized

Figure 8 shows that $\Delta L/L$ at first increases with delay time after the illumination pulse and then decreases. We have interpreted the cutoff as the onset of spin-lattice relaxation. From the lowest temperature data we find that at times less than T_1 , $\Delta L/L$ increases monotonically and approximately logarithmically with time. We interpret the spin dependence as nonradiative recombination at dangling bonds. Our model is that at low temperature the nonradiative recombination occurs by tunneling of a conduction band-tail electron to the randomly dispersed dangling bonds. In this section we calculate the time dependence of $\Delta L/L$ for this model.

When there are competing radiative and nonradiative rates P_R and P_{NR} , the luminescence decay is given by

$$L(t) = L_0 \exp[-t(P_R + P_{NR})]. \quad (8)$$

If δP_{NR} is the spin-dependent change in P_{NR} , and P_R is assumed constant, then the resulting change ΔL in L is given by

$$\frac{\Delta L(t)}{L(t)} = -t \delta P_{NR}. \quad (9)$$

This result must be averaged over an appropriate distribution of radiative and nonradiative rates. Both terms are expected to have a very broad distribution because of the $\exp(-2\alpha R)$ term in the tunneling rate. Therefore, to a good approximation the luminescence at decay time t is dominated by events for which

$$P_R + P_{NR} \approx 1/t. \quad (10)$$

In addition, if $P_{NR} \gg P_R$, then the recombination is predominately nonradiative and so does not contribute much to the luminescence. We therefore make the approximation that the luminescence is entirely determined by events for which

$$\begin{aligned} P_R &= 1/t, \\ P_{NR} &< 1/t, \end{aligned} \quad (11)$$

Following the analysis of Kaplan *et al.*,²¹ we also assume that

$$\delta P_{NR} = \beta P_{NR}, \quad (12)$$

where β is a constant. This seems to be the most physically reasonable assumption and is justified by the fact that the overlap factor $\exp(-2\alpha R)$ must be present in the rate regardless of the spin orientation.

$\Delta L/L$ is then found by summing the different contribution given by Eq. (9) over the values of P_R and P_{NR} in Eq. (11),

$$\frac{\Delta L(t)}{L(t)} = \frac{-\beta t \int_0^{1/t} G(P_{NR}) P_{NR} dP_{NR}}{\int_0^{1/t} G(P_{NR}) dP_{NR}}, \quad (13)$$

where $G(P_{NR})$ is the distribution function for P_{NR} . For the assumed random distribution, recombination will occur at the nearest-neighbor dangling bond whose distance R has the distribution

$$F(R) = 4\pi R^2 N \exp\left[-\frac{4\pi R^3 N}{3}\right], \quad (14)$$

where N is the density of centers. F and G are related by

$$P_{NR} = \omega_0 \exp(-2\alpha R). \quad (15)$$

Equation (13) then becomes

$$\begin{aligned} \frac{\Delta L(t)}{L(t)} &= -4\pi\omega_0 N \beta t \exp\left[\frac{4\pi R_t^3 N}{3}\right] \\ &\times \int_{R_t}^{\infty} R^2 \exp\left[-2\alpha R - \frac{4\pi R^3 N}{3}\right] dR, \end{aligned} \quad (16)$$

where

$$2\alpha R_t = \ln(\omega_0 t). \quad (17)$$

We next note that over the time interval of interest, $10^{-6} - 10^{-2}$ sec, $2\alpha R_t$ ranges from 14 to 23, assuming $\omega_0 = 10^{12}$ sec⁻¹. On the other hand, for $N = 3.5 \times 10^{17}$ cm⁻³ the term $4\pi R^3 N/3$ ranges from 0.5 to 2.2. Thus, the integral is dominated by the first term in the exponent. Accordingly, we approximate the integral by setting $R = R_t$ in the second term and so obtain

$$\frac{\Delta L(t)}{L(t)} = \frac{\pi N \beta}{2\alpha^3} [(\ln \omega_0 t)^2 + 2 \ln \omega_0 t + 2]. \quad (18)$$

A numerical integration of Eq. (16) confirms that this expression is a reasonable approximation to the integral.

These results show that the distribution of lifetimes weakens the time dependence predicted by Eq. (9) and gives an approximately logarithmic dependence as observed. The data of Fig. 8 in fact decrease at short times faster than predicted by Eq.

(8). It is not clear whether this is due to a smaller value of ω_0 , to microwave effects (note that the plots of $\Delta L/L$ versus rf power change with delay time), or to the approximations introduced in the calculation. Nevertheless, we conclude that the data are in general agreement with the model of nonradiative tunneling at randomly distributed centers.

Setting $\alpha^{-1} = 10 \text{ \AA}$ in addition to the parameters given above,⁶ we find that at 10^{-3} sec, from Eq. (18)

$$\Delta L/L = 0.25\beta, \quad (19)$$

compared to an observed value of ~ 0.03 . The difference between these values presumably arises either because β is small or because the line is inhomogeneously broadened, so that only $\sim 10\%$ of spins are in resonance at one time (see Sec. V B).

D. Time-resolved ODMR when only one spin is thermalized

According to our interpretation of the dangling-bond ODMR results, the value of T_1 for the band-tail electrons should be long, greater than 10^{-2} sec at 15 K. On the other hand, T_1 for holes appears to be small, $\sim 10^{-5}$ sec at 15 K (see Sec. V E). It is, therefore, of interest to analyze the time-resolved ODMR to cover the time interval when only one spin relaxes. We adopt a simple model in which the exchange coupling is sufficiently small that the spins can be considered as effectively independent, and the pairs are either parallel (*P*) or antiparallel (*A*) depending on their relative orientation, and we assume that only antiparallel pairs recombine. The rate diagram is shown in Fig. 16 where q is the spin-lattice relaxation rate (T_1^{-1}) and s is the recom-

bination rate. Since the pairs can be created with either orientation to the magnetic field, the energy ordering varies from site to site. In the absence of recombination the T_1 process results in equal average occupation of the two levels. However, recombination depletes the *A* level which is restored to an equal population by microwave resonance, resulting in ODMR.

An analysis of the rate equation for the model of Fig. 16 is straightforward, and the result depends on the initial conditions. We consider first a geminate process for which $N_1 = N_0$ and $N_2 = 0$ at $t = 0$. We obtain

$$\frac{N_1(t)}{N_2(t)} = \frac{(\Gamma^2 + 1)^{1/2}(e^{2\delta} + 1)}{(e^{2\delta} - 1)} - \Gamma, \quad (20)$$

where

$$\Gamma = s/2q \text{ and } \delta = t[s^2 + (q/2)^2]^{1/2}.$$

Since we are dealing with a broad distribution of decay times, at each measurement time the luminescence is dominated by decay processes for which $s \approx 1/t$, as discussed in Sec. V C. Using this approximation and setting $q = 1$ to define the time scale in units of T_1 results in N_1/N_2 , as shown in Fig. 16. (Note that Fig. 16 actually plots $1 - N_1/N_2$.) N_1/N_2 is greater than unity at times up to $0.8T_1$. For a radiative process, this results in quenching ODMR with unthermalized spins. At longer times N_1/N_2 drops below unity, reaches a minimum near $2T_1$, and then converges towards unity. Thus we expect an enhancing ODMR effect in the time range from T_1 to about $10T_1$.

A similar analysis of a nongeminate process is also shown in Fig. 16. For this case the initial conditions are $N_1 = N_2 = N_0/2$. As expected, there is no quenching ODMR ($N_1/N_2 > 1$) at short times, but instead an enhancing effect ($N_1/N_2 < 1$) which disappears slowly above T_1 .

The data of Fig. 12 show an enhancing line E_1 that turns on at a time $\sim 30 \mu\text{sec}$ at 15 K decreasing to $\sim 7 \mu\text{sec}$ at 50 K. In each case the enhancing line is seen over about one decade in time. The turn on time agrees well with other estimates of T_1 for the broad hole resonance (see Sec. V E) and so the data are qualitatively in agreement with the geminate recombination model. The expected asymmetry in N_1/N_2 (see Fig. 16) is not observed in the data, but we believe this could be explained by the approximations introduced into the model or by some distribution in the T_1 values. The nongeminate model does not give such a good qualitative description of the data. Although the evidence

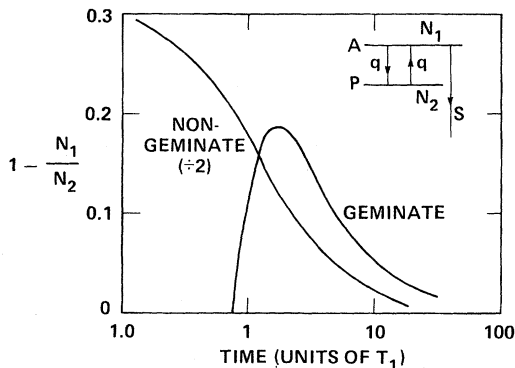


FIG. 16. Population difference $1 - N_1/N_2$ as a function of time for the model described in the text.

therefore favors the geminate process, it should be noted that the geminate process predicts a quenching line at short times. Although we do in fact observe such a quenching effect Q_2 (see Fig. 12), the microwave pulsing experiments show that the electron component of this line is nonradiative, and we have instead identified this as the Auger mechanism. Because the hole line appears in both quenching and enhancing signals, we cannot determine if any part of the quenching signal is from the radiative process.

E. Spin-lattice relaxation times

In this section we discuss the various ODMR and ESR measurements of T_1 , first for Q_1 in high-defect-density samples and second for E_1 in the low-defect-density material. As described in Sec. VC, the time-resolved measurement of Q_1 exhibit a cutoff which is interpreted as a spin-lattice relaxation effect from which T_1 can be obtained. T_1 can also be estimated from the microwave saturation of the usual dangling bond ESR as described elsewhere.¹⁸ These data are compared in Fig. 17. The relatively good agreement within the anticipated uncertainty leads us to deduce that the ODMR is in fact measuring T_1 of the dangling bonds. Since the ODMR measures the shorter T_1 of the two states involved in the resonance, we deduce that the band-tail electrons have T_1 which is at least as long, although there is no further evidence as to its actual magnitude.

For the enhancing line E_1 , ODMR provides two methods of determining T_1 . Firstly, the light pulsing measurements conform to the predictions discussed in Sec. VD. We therefore obtain T_1 from the onset time of E_1 which we chose to be the time at which $\Delta L/L$ is half its maximum value for t_1 . Secondly, T_1 is also found from the microwave pulsing experiments at the turnoff of the pulse (see Fig. 14). Since the negative transient has a time constant which is much faster than the decay during the pulse, we interpret the faster time as T_1 , following the arguments given in Sec. IIA. Relaxation of the spins causes the negative transient at the end of the pulse. In this case signal-to-noise limitations, and separating the effects of T_1 and the recombination time, restrict the time resolution to about a factor of 2. We have also estimated T_1 from the ESR saturation of the hole line in light-induced ESR. This experiment is difficult because of the small signal, but T_1 can be found over a limited temperature range.

The T_1 values from these three techniques are shown in Fig. 17. The good agreement gives confidence in the values and also extra confidence in the interpretation of the time-resolved ODMR data. For example, if we interpreted E_1 as a nongeminate process (see Sec. VD), then our estimate of T_1 would be approximately five times larger and not in agreement with the other methods.

It is of interest to compare the T_1 values for dangling bonds T_1^D and holes T_1^h . At 15 K, T_1^D is 3 orders of magnitude larger than T_1^h . T_1^D varies as T^{-2} above ~ 100 K, whereas T_1^h has a T^{-1} dependence. Evidently the dangling bonds relax through a Raman process, while the holes relax by a single-phonon direct process.

The interpretation of T_1 measurements is complicated by many different processes, and no calculations for the case of *a*-Si:H have been performed. Commonly, the direct process is observed at low temperature with a transition to the Raman process as the temperature is raised. For example, the crossover occurs at 2 K for donors in crystalline Si, with T_1 values of 10^3 sec.²⁵ The Raman process is observed for the positive divacancy with T_1 of 10^{-3} sec at 20 K,²⁶ which is a comparable magnitude to the dangling-bond data in Fig. 17. On the other hand, the direct process we observe for holes is 7 orders of magnitude faster than donors and at

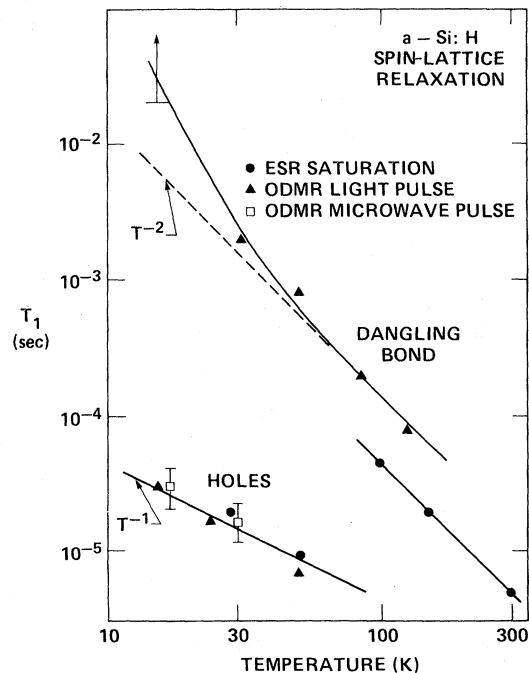


FIG. 17. Measurements of the spin-lattice relaxation time for dangling bonds and band-tail holes from ODMR and ESR.

least 3 orders of magnitude faster than for the divacancy in crystalline Si. A detailed calculation of T_1 as well as improved data for *a*-Si:H would be most valuable to understand this difference in the values.

F. Summary

We report the spin dependence of recombination in undoped *a*-Si:H. Of all the techniques used, time-resolved measurements seem to be the most informative in understanding the effects. We find three distinct spin-dependent processes with the following characteristics.

Q_1 line. This line is seen predominantly in samples with a high dangling-bond density ($> 10^{17}$ cm⁻³). The quenching effect occurs at unthermalized spins characterized by a relatively long T_1 ranging from $\sim 10^{-4}$ sec at 100 K to $> 2 \times 10^{-2}$ sec at 15 K. The spin dependence occurs at nonradiative recombination events. The ODMR line shape is interpreted as a combination of the dangling bond and conduction-band-tail resonances. Nonradiative recombination by tunneling of an electron into a dangling band readily accounts for all the features of the ODMR effect.

Q_2 line. Q_2 is a different quenching line observed in samples with a low-spin density. It is associated with unthermalized spins, but in this case the effective T_1 is rather short, being 2×10^{-5} sec at 20 K. The effect occurs through nonradiative recombination as for Q_1 . The ODMR line shape identifies the

particles as electrons and holes in band-tail states. We interpret the effect as the nonradiative Auger process which has been identified previously in luminescence experiments.

E_1 line. The enhancing line is seen most readily in samples of low-defect density and is associated with a radiative transition. The time-resolved properties indicate that E_1 occurs at a geminate pair when one spin is thermalized and the other is not. The ODMR line shape is not readily identifiable from ESR. We suggest that it arises from the band-tail electron and hole lines which are "averaged," possibly by an exchange interaction.

The ODMR data is found to be consistent with and generally supportive of the recombination models we have previously suggested from luminescence data. The nonradiative recombination at dangling bonds is particularly clearly seen in ODMR. Further studies are needed to clarify the interpretation of Q_2 and E_1 , particularly the latter. A useful result of the time-resolved ODMR is the measurement of spin-lattice relaxation times, which we report for dangling bonds and band-tail hole states.

ACKNOWLEDGMENTS

The author is very grateful to D. K. Biegelsen, B. C. Cavenett, and S. Depinna for helpful discussion, and to J. Zesch for expert technical assistance. The work is partially supported by the Solar Energy Research Institute under Contract No. XJ-0-9097-1.

¹See R. A. Street, *Adv. Phys.* **30**, 593 (1981).

²R. Fischer, W. Rehm, J. Stuke, and U. Voget-Grote, *J. Non-Cryst. Solids* **35-36**, 687 (1980).

³D. Engemann and R. Fischer, *Phys. Status Solidi B* **79**, 195 (1977).

⁴C. Tsang and R. A. Street, *Phys. Rev. B* **19**, 3027 (1979).

⁵R. A. Street, *Philos. Mag. B* **37**, 35 (1978).

⁶R. A. Street, J. C. Knights, and D. K. Biegelsen, *Phys. Rev. B* **18**, 1880 (1978).

⁷R. A. Street, *Phys. Rev. B* **23**, 861 (1981).

⁸W. Rehm, R. Fischer, J. Beichler, and W. Siebert, *J. Phys. Soc. Jpn.* **49**, Suppl. A, 1209 (1980).

⁹M. H. Brodsky and R. S. Title, *Phys. Rev. Lett.* **23**, 581 (1969).

¹⁰R. A. Street and D. K. Biegelsen, *Solid State Commun.* **33**, 1159 (1980).

¹¹M. A. Paesler and W. Paul, *Philos. Mag. B* **41**, 393 (1980).

¹²S. Depinna and B. C. Cavenett, *Solid State Commun.* **41**, 263 (1982); *Philos. Mag.* (in press).

¹³B. C. Cavenett, *Adv. Phys.* **30**, 475 (1981).

¹⁴K. Morigaki, D. J. Dunstan, B. C. Cavenett, P. Dawson, and J. E. Nicholls, *Solid State Commun.* **26**,

981 (1978).

¹⁵D. K. Biegelsen, J. C. Knights, R. A. Street, C. Tsang, and R. M. White, *Philos. Mag. B* **37**, 477 (1978).

¹⁶S. Depinna and B. C. Cavenett, *Proceedings of the Ninth International Conference on Amorphous and Liquid Semiconductors* (in press).

¹⁷K. Morigaki, Y. Sano and I. Hirabayashi, *Solid State Commun.* **39**, 947 (1981).

¹⁸R. A. Street, D. K. Biegelsen, and J. Zesch *Phys. Rev. B* **25**, 4334 (1982).

¹⁹D. J. Dunstan and J. J. Davies, *J. Phys. C* **12**, 2927 (1979).

²⁰See D. K. Biegelsen, *Sol. Cells* **2**, 421 (1980).

²¹D. Kaplan, I. Solomon, and N. F. Mott, *J. Phys. (Paris)* **19**, L51 (1978).

²²J. S. Hyde, *Phys. Rev.* **119**, 1492 (1960).

²³J. J. Davies, *J. Phys. C* **11**, 1907 (1978).

²⁴See for example, G. Feher, *Phys. Rev.* **114**, 1219 (1959).

²⁵T. G. Castner, *Phys. Rev.* **130**, 58 (1963).

²⁶C. A. J. Amermerlaan and A. van de Wiel, *J. Magn. Reson.* **21**, 387 (1976).